Periodicity and Chaos in Chemiluminescence: The Ruthenium-Catalyzed Belousov−Zhabotinsky Reaction

K.-P. Zeyer[†] and F. W. Schneider*

Institut für Physikalische Chemie der Universität Würzburg, Am Hubland, 97074 Würzburg, Germany

Received: June 2, 1998; In Final Form: August 26, 1998

We investigate the chemiluminescence of the homogeneous Belousov−Zhabotinsky (BZ) reaction catalyzed by tris(2,2'-bipyridine)ruthenium (II) ($[Ru(bpy)_3]^{2+}$) in a continuous-flow stirred tank reactor where the chemiluminescence originates from the electronically excited $[Ru(bpy)_3]^{2+}$ catalyst. At high flow rates, Farey-ordered as well as complex burst-like states are observed in the pure ruthenium-catalyzed reaction which we investigated using five different concentration sets. We also characterized the chemiluminescent behavior when both Ru^{2+} and Ce^{3+} were present at four different mole fractions. Under conditions of low Ru^{2+} concentrations, we observed two chaotic chemiluminescent states which are reached by a period-adding and a period-doubling route, respectively. Model calculations with the reaction scheme of Gao and Försterling were performed with semiquantitative agreement with our experimental observations.

Introduction

The ruthenium-catalyzed Belousov−Zhabotinsky (BZ) reaction[1] is a BZ variant which shows chemiluminescence (CL)[2] and which interacts with visible light.[3] Perturbation with an external light source changes the periods of oscillations, produces oscillations from steady states (rhythmogenesis),[4] or annihilates the oscillations (phase death).[5] This light-sensitive reaction can also be used in spatially distributed systems to encode images by partial illumination[6] or to anchor and modulate spiral waves.[7] Earlier, steady-state chemiluminescence was observed by Hercules and Lytle[8] by reducing $[Ru(bpy)_3]^{3+}$ with sodium hydroxide. The spectra of the chemiluminescence and the photoluminescence of the corresponding $[Ru(bpy)_3]^{2+}$ complex appear to be identical which indicates that the chemiluminescence occurs from an electronically excited state of the $[Ru(bpy)_3]^{2+}$ complex which is located 2.12 eV above the ground state.[2,8] The same type of chemiluminescence was observed in the synproportionation reaction of $[Ru(bpy)_3]^{3+}$ and $[Ru(bpy)_3]^{1+}$[9] and in reduction reactions of $[Ru(bpy)_3]^{3+}$ by organic acids such as pyruvic, lactic, or malonic acid.[10] Bolletta and Balzani[2] observed transient oscillatory chemiluminescence when the BZ reaction was run in a closed reactor with $[Ru(bpy)_3]^{2+}$ as a catalyst. These authors showed that the chemiluminescence oscillates in phase with the oscillations of the Ru^{3+}-concentration although the CL intensity is much too low to be seen with the naked eye. However, it can easily be detected with a sensitive photomultiplier.

All these latter measurements were performed in the batch. There are only a few investigations of chemiluminescence in the open system.[11] To thoroughly characterize this chemiluminescent reaction we undertook a systematic study over a wide range of concentrations and residence times in a continuous-flow stirred tank reactor (CSTR). One set of concentrations corresponds to those given by Bolletta and Balzani,[2] and two other sets correspond to sets that are used in the cerium-catalyzed BZ reaction where complex periodic and chaotic dynamics are observed in the Ru-free nonchemiluminescent system.[12−15] Since we did not observe any chaotic states in the pure ruthenium reaction, we added Ce^{3+} in various proportions in order to determine the approximate onset of chaos. In the course of these studies we discovered two chaotic states which are reached via a period-adding and a period-doubling route, respectively, at a high mole fraction of cerium (95 mol %). We performed model calculations with the model of Gao and Försterling[16] which we slightly extended. The model is based on the Radicalator scheme[17] of the BZ dynamics. When the experimental time-dependent chemiluminescence was equated with the Ru^{3+} concentrations as calculated by the model, semiquantitative agreement between the model and our CSTR experiments was obtained.

Experimental Section

Experimental Setup. The reactor consists of a quartz glass cuvette of 3.43 mL volume. The reaction solutions enter the reactor through the top via three Teflon tubes. These tubes end just above a Teflon stirrer which is rotated magnetically at a stirring rate of 800 rpm. The reactor is placed in a dark-box to prevent external light from entering. A precise syringe pump delivers the reaction solutions through three glass syringes.The syringes, the feed lines, and the reactor box are thermostated at 28.0 ± 0.1 °C. The total emitted light (λ_{max} = 620 nm) from the front window of the cuvette is measured by a photomultiplier (Thorn Emi). To reduce the inherent noise level, the photomultiplier was cooled to −30 °C with a Peltier element. We used 1100 and 1200 V as cathode voltages. The photomultiplier potentials were amplified and stored on a computer with sampling rates ranging from 1 to 10 Hz. Altogether, over 250 runs which lasted between 2 and 20 h each were performed.

Materials. Sulfuric acid (Riedel de-Haën), sodium bromate (Merck), $Ce_2(SO_4)_3$ (Fluka), and $[Ru(bpy)_3]Cl_2 \cdot 6H_2O$ (Strem) were used without further purification. The malonic acid (Merck-Schuchardt) was recrystallized twice from acetone to remove trace impurities.[18] The reaction solutions were prepared with highly purified water (Milli-Q, Millipore; specific resistance

* Author to whom correspondence should be addressed.
[†] Present address: Max-Planck-Institut für Dynamik komplexer technischer, Systeme, Leipziger Str. 44, 39120 Magdeburg, Germany.

10.1021/jp982454c CCC: $15.00
Published on Web 10/30/1998

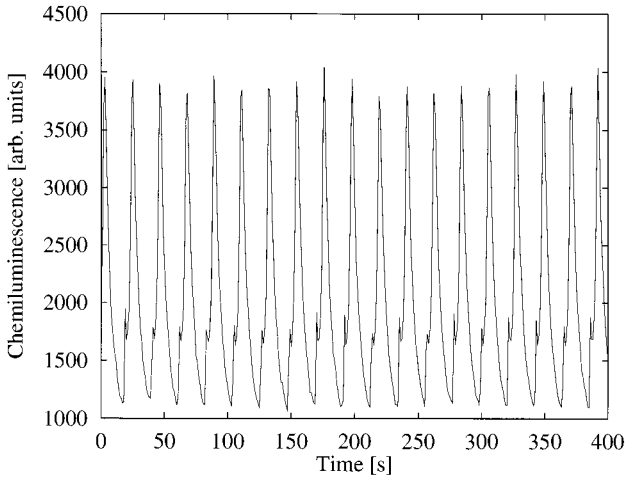

Figure 1. Concentration set 1: Chemiluminescence intensity versus time at $k_f = 6.3 \times 10^{-3}$ s^{-1} ($\tau = 2.6$ min): periodic P2 are observed.

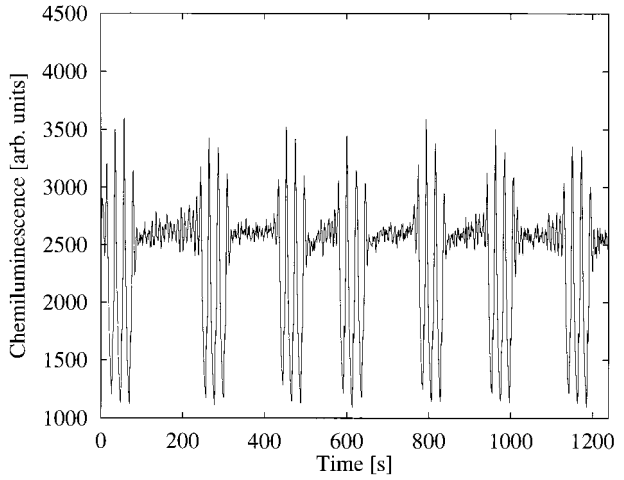

Figure 2. Concentration set 1: Chemiluminescence intensity versus time at $k_f = 8.9 \times 10^{-3}$ s^{-1} ($\tau = 1.9$ min): Burst-like oscillations with four large excursions per oscillation cycle.

> 10 MΩ·cm). The water was equilibrated with air. The three feed lines contain the following solutions. Concentration set 1 was $[(COOH)_2CH_2] = 0.75$ M (syringe 1), $[H_2SO_4] = 3.00$ M and $[Ru(bpy)_3]Cl_2 \cdot 6H_2O = 3.0 \times 10^{-4}$ M (syringe 2), and $[NaBrO_3] = 0.18$ M (syringe 3); concentration set 2: $[(COOH)_2CH_2] = 0.75$ M, $[H_2SO_4] = 0.60$ M and $[Ru(bpy)_3]Cl_2 \cdot 6H_2O = 2.5 \times 10^{-3}$ M, and $[NaBrO_3] = 0.30$ M; concentration set 3: $[NaBrO_3] = 0.42$ M; concentration set 4: $[NaBrO_3] = 0.75$ M; and concentration set 5: $[NaBrO_3] = 1.50$ M. In concentration sets 2−5, only the bromate concentration was varied. To obtain reactor concentrations divide by three.

The Gao and Försterling Model. Gao and Försterling[16] proposed a model for the ruthenium-catalyzed BZ reaction with bromomalonic acid as an organic substrate. The model consists of 19 reaction steps and 16 variables (Table 1). Two negative feedback loops are contained in the model. The first is the reaction of bromide with bromous acid (step 2, Table 1) and the second loop involves the reaction of organic radicals with $BrO_2\cdot$ radicals (step 14; Table 1).[16] To account for malonic acid as an organic substrate we added steps 17, 18, and 19 (Table 1) in analogy to steps 11, 12, and 13 of the original model.[19] Reactions between $[Ru(bpy)_3]^{3+}$ and malonic acid were neglected since they are less important than those in the cerium-catalyzed BZ reaction.[19] The rate constants were taken from refs 16 and 20. The numerical integration of the model equations was performed with the Livermore solver of ordinary differential equations (LSODE)[21] on a SGI−Irix computer.

Experimental Results

The Ruthenium-Catalyzed BZ Reaction without Cerium. *Concentration Set 1.* Using concentration set 1 of Bolletta and Balzani[2] we exclusively obtained period-1 (P1) chemiluminescent oscillations from $k_f = 1 \times 10^{-4}$ s^{-1} (residence time $\tau =$ 166.7 min) to 2.1×10^{-3} s^{-1} ($\tau = 2.1$ min). The oscillation periods T display a maximum ($T = 26.8$ s at $k_f = 3.1 \times 10^{-3}$ s^{-1} ($\tau = 5.3$ min)). At high flow rates (above $k_f = 2.1 \times 10^{-3}$ s^{-1} ($\tau = 7.9$ min)) the oscillations show a small shoulder (period-2, one large and one small oscillation) (Figure 1) which was already seen by Bolletta and Balzani[2] in the closed system and attributed to the reduction of $[Ru(bpy)_3]^{3+}$ by organic radicals to produce the excited Ru(II) complex.[22] At still higher flow rates above 8.1×10^{-3} s^{-1} ($\tau = 2.1$ min) complex oscillations were observed which are composed of small and large burst-like oscillations. Here, the number of large oscillations decreases and the number of small oscillations increases with increasing flow rate. The time series at $k_f = 8.9 \times 10^{-3}$ s^{-1} ($\tau = 1.9$ min) displays four spikes per oscillation cycle (Figure 2). Irregularities in the distribution of the high-amplitude bursts are attributed to experimental noise. This interpretation is based on our data analysis such as attractor reconstruction and one-dimensional maps. The oscillations vanish and give way to a steady state at $k_f \geq 9.9 \times 10^{-3}$ s^{-1} ($\tau \leq 1.7$ min). The bifurcation diagram is given in Figure 3.

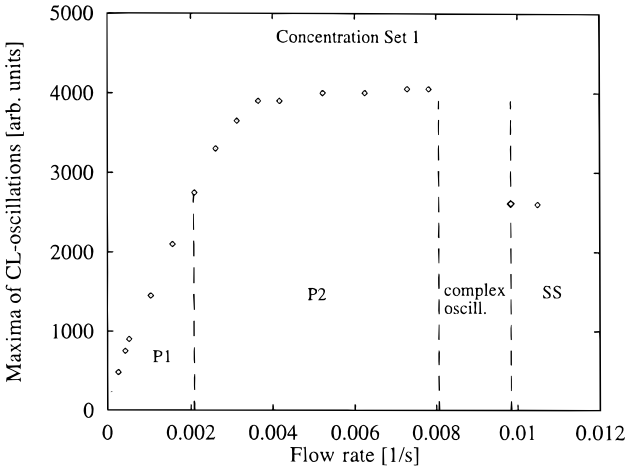

Figure 3. Concentration set 1: Experimental bifurcation diagram: Maxima of the oscillations/SS versus flow rate: P1 and P2 oscillations, complex oscillations, and steady state (SS). The chemiluminescence minima are not shown.

Concentration Sets 2 and 3. Since we did not find any chaotic dynamics under the conditions of Bolletta and Balzani[2] (concentration set 1), we decided to investigate two further concentration sets at which the cerium-catalyzed BZ reaction (without Ru) is known to display deterministic chaos.[12−15] Using concentration set 2 we only found P1 oscillations at all flow rates (from $k_f = 1.4 \times 10^{-4}$ s^{-1} ($\tau = 119.0$ min) to 3.7×10^{-4} s^{-1} ($\tau = 45.0$ min)) (not shown). For concentration set 3, a relatively broad deterministic chaotic region exists in the pure cerium-catalyzed BZ reaction.[15] However, the pure Ru^{2+} chemiluminescent reaction shows only P1 oscillations at flow rates below 6.3×10^{-3} s^{-1} ($\tau = 2.6$ min). In a plot of the oscillation period versus the flow rate, the period of the P1 oscillations displays a maximum at $k_f = 3.1 \times 10^{-3}$ s^{-1} ($\tau =$ 5.4 min) (Figure 4a). At higher flow rates we found P2 ($k_f =$ 7.3×10^{-3} s^{-1}; $\tau = 2.3$ min) (Figure 5) and P3 ($k_f = 8.3 \times$

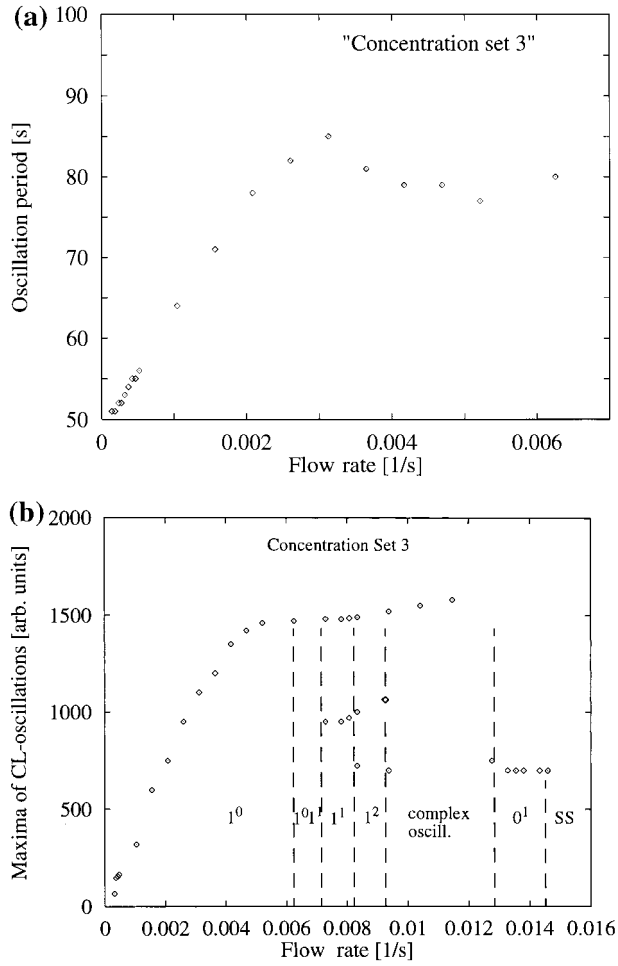

Figure 4. (a) Concentration set 3: Oscillation period versus flow rate: the oscillation period passes through a maximum at $k_f = 3.1 \times 10^{-3}$ s^{-1}. (b) Concentration set 3: Experimental bifurcation diagram: oscillation amplitude versus flow rate, see text. SS is located at about the same level as 0^1.

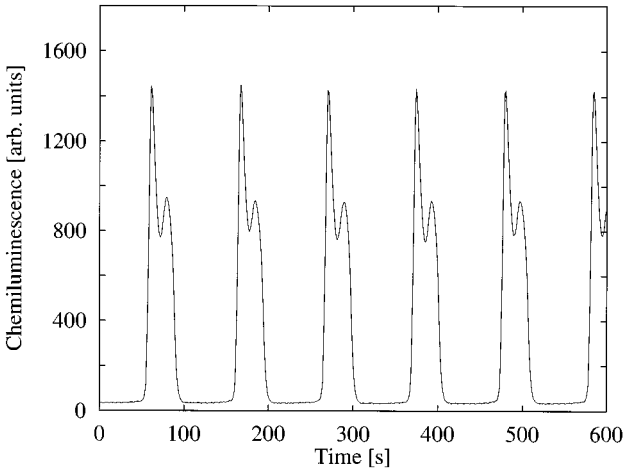

Figure 5. Concentration set 3: P2 (1^1) oscillations at $k_f = 7.3 \times 10^{-3}$ s^{-1} ($\tau = 2.3$ min).

10^{-3} s^{-1}; $\tau = 2.0$ min) (Figure 6) oscillations. When the numbers of large oscillations and small oscillations are specified by L and S, respectively, an oscillating state may be described as L^s. Thus, the P1 state may be denoted by 1^0 and the P2 state 1^1. At 6.8×10^{-3} s^{-1} we observed a concatenated 1^01^1 pattern (between a 1^0 and 1^1 state) as part of a Farey[23] sequence (Figure 7). When the flow rate is further increased, complex

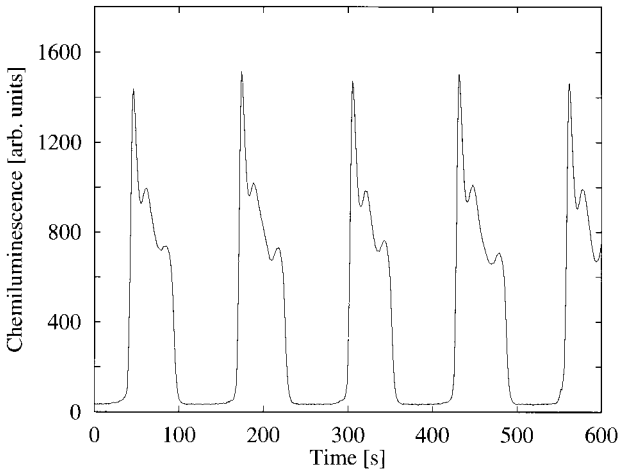

Figure 6. Concentration set 3: P3 (1^2) oscillations at $k_f = 8.3 \times 10^{-3}$ s^{-1} ($\tau = 2.0$ min).

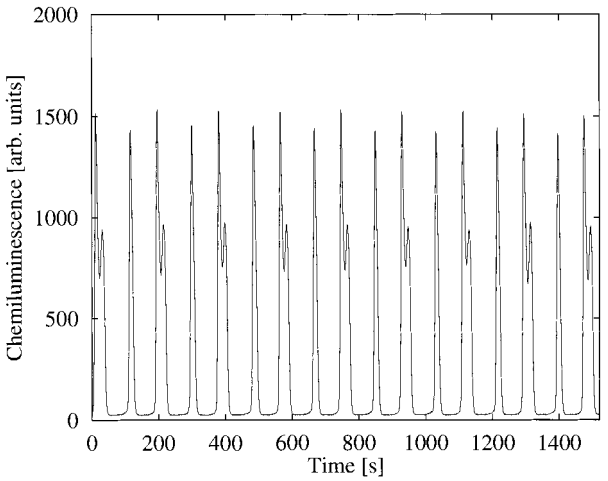

Figure 7. Concentration set 3: Concatenated 1^01^1-oscillations (between a 1^0 and 1^1 state) at $k_f = 6.8 \times 10^{-3}$s^{-1} ($\tau = 2.5$ min).

oscillations with higher periods emerge which could not be resolved any further. Finally, 1^0 oscillations with small amplitudes follow in a flow rate interval (from $k_f = 1.27 \times 10^{-2}$ s^{-1} ($\tau = 1.3$ min) to 1.45×10^{-2} s^{-1} ($\tau = 1.2$ min)) which give way to a steady state SS at a higher flow rate of $k_f > 1.45 \times 10^{-2}$ s^{-1}. These observations are summarized in a bifurcation diagram (Figure 4b).

Concentration Sets 4 and 5. We further searched for chaotic dynamics at higher bromate concentrations in the pure Ru^{2+} reaction. Using concentration sets 4 and 5 we investigated the flow rate intervals between $k_f = 1.6 \times 10^{-4}$ s^{-1} ($\tau = 104.2$ min) and $k_f = 6.3 \times 10^{-3}$ s^{-1} ($\tau = 2.6$ min). In both cases we only found P1 (1^0) oscillations. For concentration set 4, the oscillation periods increase with increasing flow rate up to $T =$ 65 s at $k_f = 6.25 \times 10^{-3}$ s^{-1} while for concentration set 5 a strong decline of the periods occurs first (T_{min} =16 s at $k_f = 2.1 \times 10^{-3}$ s^{-1}) which is followed by a small increase (T_{max} =18 s at $k_f = 6.25 \times 10^{-3}$ s^{-1}). In general, higher bromate concentrations show shorter oscillation periods.

Experiments with $[Ru(bpy)_3]SO_4$. To ascertain that the observed lack of aperiodic behavior in the pure Ru^{2+} system is not due to the use of the chloride salt of the ruthenium catalyst we converted the chloride to the sulfate.[16,24] An amount of 1.0 g (1.34 mmol) of $[Ru(bpy)_3]Cl_2 \cdot 6H_2O$ was dissolved in 16 mL of water. Forty milliliters of 5 M sulfuric acid was added and the sulfate precipitated. After 24 h the precipitate was filtered

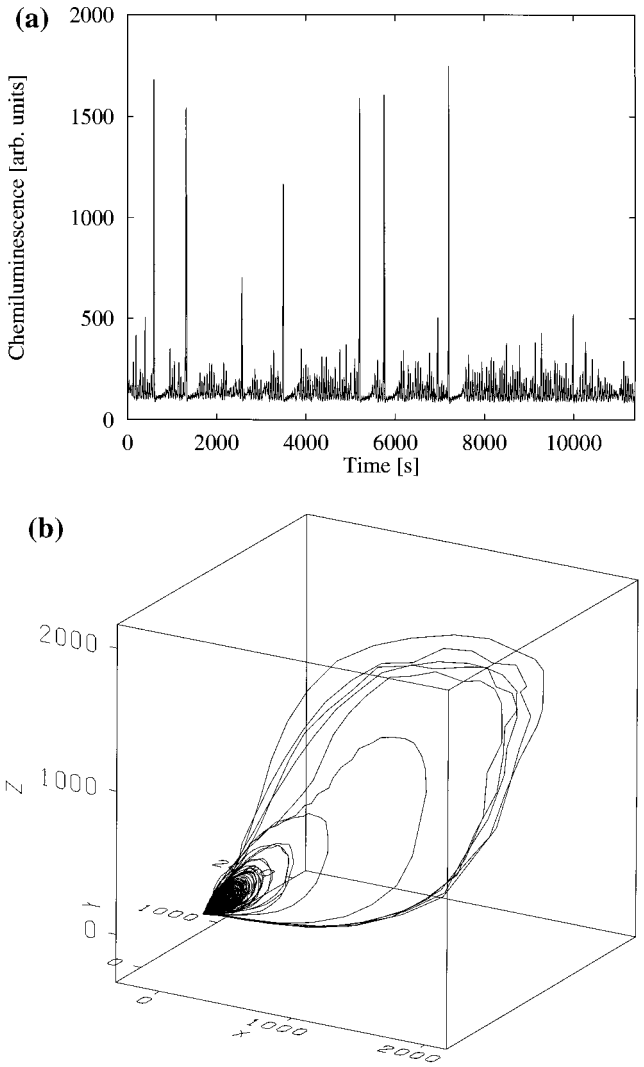

Figure 8. (a) Chaotic time series (C1) at $k_f = 1.28 \times 10^{-3}$ s^{-1} (τ = 13.0 min) reached by a period-adding route, mixed catalysts, mole fraction $Ru^{2+} = 0.05$. (b) Attractor of C1 obtained from Figure 8a with the Takens delay method. Delay time: 3 s.

and washed with 96% ethanol and ether. After drying at 50 °C for 2 days, the sulfate (662.4 mg; $[Ru(bpy)_3]SO_4 \cdot H_2O$, 72.5%) was dissolved in 100 mL of water. The concentration of this stock solution was determined by the absorption at 452 and 460 nm with a UV−VIS spectrophotometer (Hewlett-Packard diode array spectrophotometer) using the extinction coefficients $\epsilon_{452\ nm} = 11900$ cm^{-1} and $\epsilon_{460\ nm} = 11350$ cm^{-1} (T = 23.5 °C).

We also determined the bifurcation diagram for concentration set 3 using the sulfate complex. It is similar to the chloride catalyst containing the same dynamic states (1^0, 1^1, and $1^0 1^1$). However, the oscillation amplitudes and periods are larger (by a factor of ∼1.5) than those of the chloride system and the bifurcation diagram is shifted to higher flow rates with T_{max} = 101 s at $k_f = 2.1 \times 10^{-3}$ s^{-1} (not shown).

Mixed Ruthenium and Cerium Catalysts. To characterize the mixed catalytic system we added Ce^{3+} to the Ru^{2+} catalyst, while the sum of the $[Ru(bpy)_3]^{2+}$ and Ce^{3+} concentrations was kept constant at 2.5×10^{-3} M for all four mole fractions investigated. Concentration set 3 was used for all experiments.

Mole Fraction $Ru^{2+} = 0.05$. Starting with experiments at low flow rates a chaotic state (C_1) was observed at $k_f = 1.28 \times 10^{-3}$ s^{-1} (τ = 13.1 min) (Figure 8a) which is reached by a period-adding route. Its chaotic attractor was reconstructed by the delay method according to Takens[25] and it is depicted in Figure 8b (delay time t_d = 3 s). For increasing flow rate the period-adding sequence is reversed: P5, P4, P3, and P2 states of this sequence are shown in Figure 9a−d. Higher periods could not be resolved further. The oscillation periods decrease strongly with increasing flow rate (Figure 10).

Interestingly, there is also a period-doubling sequence to chaos (C2) at the high flow rate end of the (reversed) period-adding sequence. The period-doubling starts from the P2 state with increasing flow rate (Figure 10). A P′4 state can be nicely resolved at $k_f = 4.7 \times 10^{-3}$ s^{-1} (τ = 3.55 min) (Figure 11). Chaos C2 was observed at $k_f = 4.8 \times 10^{-3}$ s^{-1} (τ = 3.47 min) (Figure 12a). The deterministic chaotic nature of this aperiodicity can be shown by its attractor (Figure 12b) which was obtained by the method of singular value decomposition (SVD-method)[26] and the corresponding one-dimensional map (Figure 12c) which displays an extremum in accordance with chaos reached by a period-doubling route. We calculated the Hausdorff dimension (D_H) of the C2 attractor as $D_H = 2.15$. Thus D_H is fractal and above 2.0 which is further evidence for the deterministic origin of the observed aperiodicity C2. The dimensional analysis was performed by the nearest neighbor method[27] (embedding dimension 15; 500 reference points). A P1 state was observed at higher flow rates ($k_f \geq 4.9 \times 10^{-3}$ s^{-1}) (Figure 10).

Mole Fraction $Ru^{2+} = 0.20$. P1 states are observed at high flow rates (not shown). With decreasing flow rate the amplitudes of the oscillations become more and more irregular until aperiodic oscillations emerge at $k_f < 1.6 \times 10^{-3}$ s^{-1} (τ > 10.4 min). This aperiodic region persists down to the lowest detection limit. We did not find any extremum in the one-dimensional maps obtained from the corresponding SVD attractor. Thus these aperiodic oscillations cannot be uniquely characterized.

Mole Fraction $Ru^{2+} = 0.50$. The dynamics are very similar to those of the mole fraction 0.20. At high flow rates P1 oscillations are observed. The amplitudes of these oscillations become irregular as the flow rate is decreased.

Mole Fraction $Ru^{2+} = 0.75$. At this high proportion of $[Ru(bpy)_3]^{2+}$ the aperiodicity described above completely vanishes and the dynamics are similar to the case of the pure ruthenium catalyst. We found P1 states exclusively in a large flow rate range (from $k_f = 5.2 \times 10^{-5}$ s^{-1} (τ = 320.5 min) to $k_f = 6.3 \times 10^{-3}$ s^{-1} (τ = 2.6 min)) (not shown).

Model Calculations without Cerium. All model calculations were performed with the extended Gao−Försterling model[16] (Table 1) which describes the pure ruthenium-catalyzed BZ reaction without the occurrence of chaos in agreement with our experiments.

Concentration Set 1. Model calculations were done in the flow rate interval from $k_f = 1.0 \times 10^{-4}$ s^{-1} (τ = 166.7 min) to 5.0×10^{-3} s^{-1} (τ = 3.3 min) in steps of 1.0×10^{-4} s^{-1}. At flow rates ≤ 4.2×10^{-3} s^{-1} ($\tau \geq$ 4.0 min) P1 oscillations emerge. The periods of these oscillations go through a maximum (T = 58 s) at $k_f = 1.8 \times 10^{-3}$ s^{-1} (τ = 9.3 min). At $k_f \geq 4.3 \times 10^{-3}$ s^{-1} ($\tau \leq$ 3.9 min) a steady state is obtained. In contrast to the corresponding experiments (Figure 2), complex periodic oscillations were not found.

Concentration Sets 2 and 3. The calculations were performed between $k_f = 1.0 \times 10^{-4}$ s^{-1} (τ = 166.7 min) and 2.0×10^{-2} s^{-1} (τ = 0.8 min) at intervals of $k_f = 1.0 \times 10^{-4}$ s^{-1}. Figure 13 shows the bifurcation diagram. The oscillation periods display a maximum (T = 223 s at $k_f = 5.9 \times 10^{-3}$ s^{-1}) as a

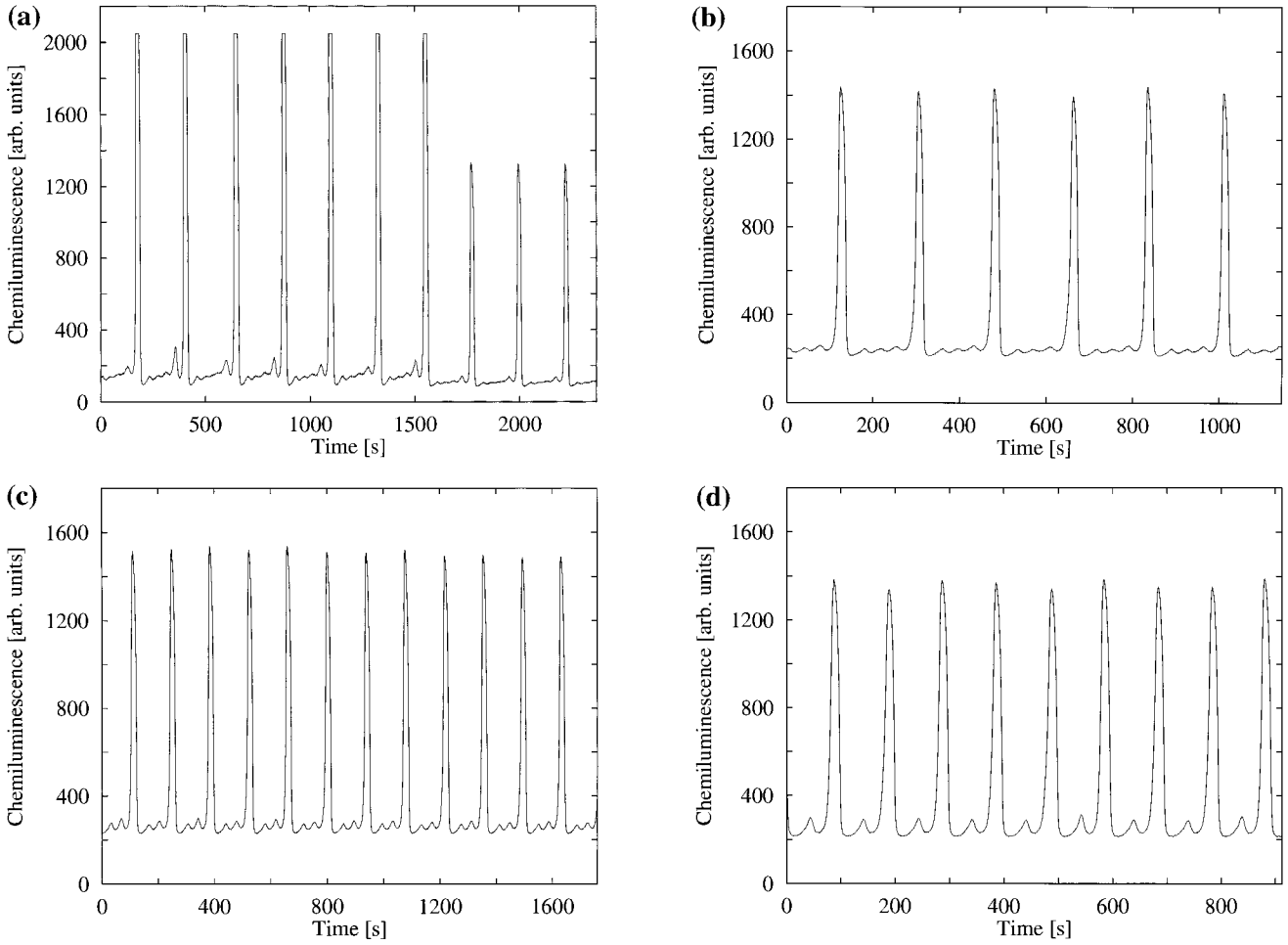

Figure 9. Mixed catalysts; mole fraction $Ru^{2+} = 0.05$: Experimental time series of the period-adding sequence: P5 state (a) the first part of Figure 9 is amplified by the factor 2.5 to facilitate the viewing of the P5 pattern, P4 state (b), P3 state (c), and the P2 state (d) at $k_f = 2.34 \times 10^{-3}$ s^{-1} ($\tau = 7.1$ min), $k_f = 2.61 \times 10^{-3}$ s^{-1} ($\tau = 6.4$ min), $k_f = 3.13 \times 10^{-3}$ s^{-1} ($\tau = 5.3$ min), and $k_f = 3.65 \times 10^{-3}$ s^{-1} ($\tau = 4.6$ min), respectively.

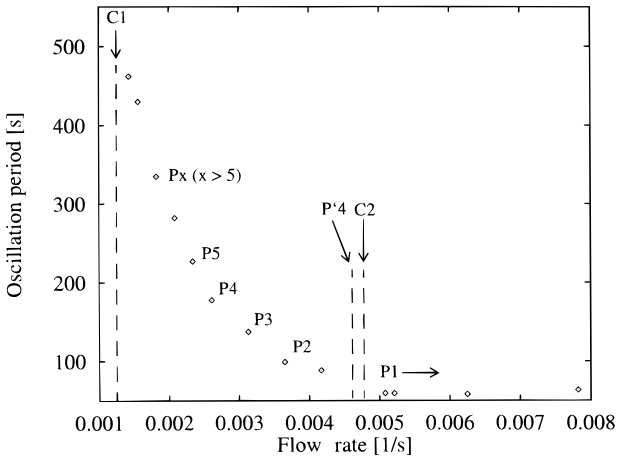

Figure 10. Oscillation periods of the period-adding sequence versus the flow rate. Mixed catalysts; mole fraction $Ru^{2+} = 0.05$. The periods increase before the onset of the period-added chaos (C_1). The labels *Px* denote the periodicity of the oscillations; where *x* is larger than 5: the exact value of *x* cannot be resolved. A period-doubled P′4-state (Figure 11) is observed at $k_f \approx 4.7 \times 10^{-3}$ s^{-1} ($T = 205$ s) which is followed by the chaotic state C2 (Figure 12) at $k_f = 4.8 \times 10^{-3}$ s^{-1}.

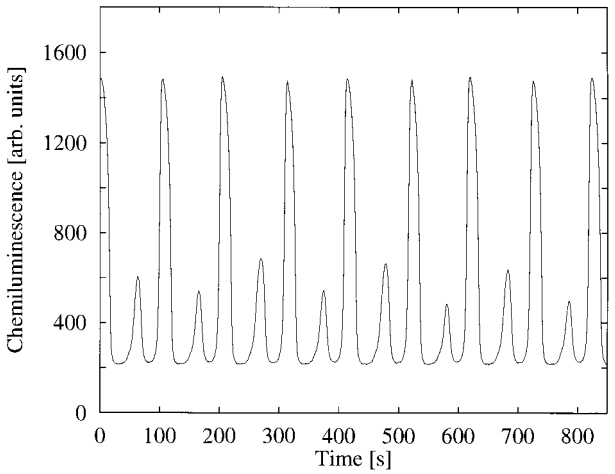

Figure 11. Mixed catalysts; mole fraction $Ru^{2+} = 0.05$: Experimental time series of P'4 state at $k_f = 4.7 \times 10^{-3}$ s^{-1} ($\tau = 3.54$ min) as part of the period-doubling sequence.

function of the flow rate as in the experiments (Figure 4a), and only P1 oscillations occur at low flow rates. At high flow rates P2 (1^1), P3 (1^2), P4 (1^3) oscillations emerge, which are separated by the concatenated states $1^0 1^1$, $1^1\ 1^2$, $1^2\ 1^3$, respectively, in accordance with a Farey sequence.[23] A P3 (1^2) state is shown in Figure 14 at $k_f = 2.2 \times 10^{-2}$ s^{-1} ($\tau = 0.76$ min) for concentration set 3. The oscillation amplitudes are very similar in both concentration sets while the oscillation periods are larger at lower bromate concentrations (maximum of the oscillation period is 295 s at $k_f = 4.9 \times 10^{-3}$ s^{-1} for concentration set 2) in semiquantitative agreement with the experiments.

Concentration Sets 4 and 5. Model calculations using concentration sets 4 and 5 were performed between $k_f = 1.0 \times$

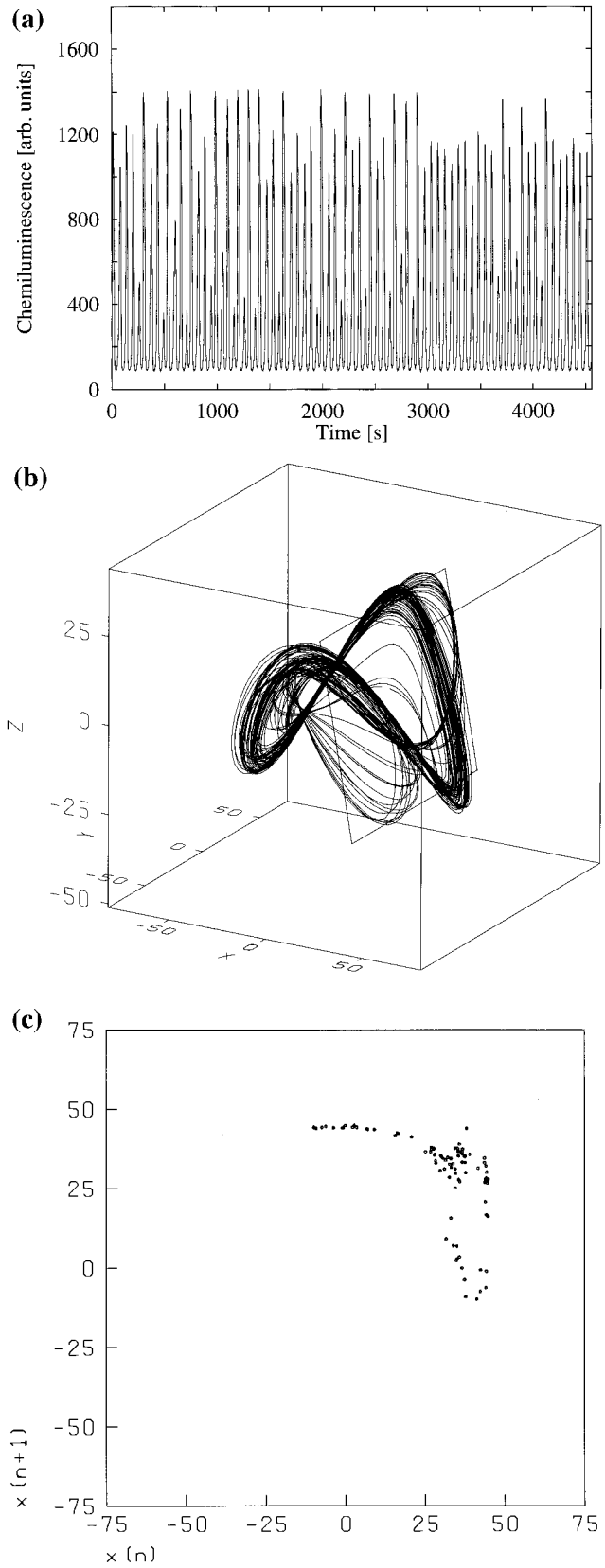

Figure 12. (a) Mixed catalysts; mole fraction $Ru^{2+} = 0.05$: Chemiluminescent chaos C2 at $k_f = 4.8 \times 10^{-3}$ s^{-1} ($\tau = 3.47$ min). (b) SVD attractor corresponding to the C2 time series (Figure 12a).The three dimensions related to the highest singular values are depicted. The Hausdorff dimension is 2.15 using the nearest neighbor method[27] (embedding dimension 15; 500 reference points) for dimensional analysis. (c) One-dimensional map obtained from the SVD attractor (Figure 12b). The extremum is characteristic for deterministic chaos originating from a period-doubling sequence.

TABLE 1: The Model according to Gao and Försterling[16] *a,b,c,d,e*

$Br^- + HOBr + H^+ \rightleftarrows Br_2 + H_2O$	(1)
$Br^- + HBrO_2 + H^+ \rightleftarrows 2HOBr$	(2)
$Br^- + BrO_3^- + 2H^+ \rightleftarrows HOBr + HBrO_2$	(3)
$HBrO_2 + H^+ \rightleftarrows H_2BrO_2^+$	(4a)
$HBrO_2 + H_2BrO_2 + \rightleftarrows HOBr + BrO_3^- + 2H^+$	(4b)
$HBrO_2 + BrO_3^- + H^+ \rightleftarrows Br_2O_4 + H_2O$	(5′)
$Br_2O_4 \rightleftarrows 2BrO_2\cdot$	(5″)
$Ru^{2+} + BrO_2\cdot + H^+ \rightleftarrows Ru^{3+} + HBrO_2$	(6)
$2BrO_3^- + 2H^+ \rightarrow HBrO_2 + HBrO_4$	(7)
$BrMA + Ru^{3+} \rightleftarrows BrMA\cdot + Ru^{2+} + H^+$	(8)
$2BrMA\cdot + H_2O \rightarrow BrMA + BrTA$	(9)
$BrTA \rightarrow MOA + Br^- + H^+$	(10)
$BrMA \rightleftarrows BrMA\text{-enol}$	(11)
$BrMA\text{-enol} + Br_2 \rightarrow Br_2MA + H^+ + Br^-$	(12)
$BrMA\text{-enol} + HOBr \rightarrow Br_2MA + H_2O$	(13)
$BrMA\cdot + BrO_2\cdot \rightarrow P$	(14)
$P \rightarrow Br^- + P_1 + H^+$	(15)
$P \rightarrow HBrO_2 + BrTA$	(16)
To account for malonic acid as the organicsubstrate we added the following steps:[19]	
$MA \rightleftarrows MA\text{-enol}$	(17)
$MA\text{-enol} + Br_2 \rightarrow BrMA + H^+ + Br^-$	(18)
$MA\text{-enol} + HOBr \rightarrow BrMA + H_2O$	(19)

[a] MA, malonic acid; BrMA, bromomalonic acid; TA, tartronic acid; BrTA, bromotartronic acid; MOA, mesoxalic acid; P and P_1, unidentified species. [b] The rate constants were chosen according to Gao and Försterling.[16] For steps 17−19 we used the following rate constants:[20] $k_{17} = 3.0 \times 10^{-3}$ s^{-1}, $k_{-17} = 2.0 \times 10^2$ s^{-1}, $k_{18} = 1.91 \times 10^6$ L mol^{-1} s^{-1}, and $k_{19} = 8.2$ L mol^{-1} s^{-1}. [c] The following initial concentrations were chosen for the variables: $[Ru^{2+}] = 5.2 \times 10^{-4}$ M and $[BrO_3^-] = 1.0 \times 10^{-2}$ M. All other variables were initialized with 1.0×10^{-8} M. [d] CSTR conditions were established by adding the term $k_f([X]_o - [X])$ to each differential equation, where k_f is the flow rate, $[X]_o$ is the inflow concentration of variable X, and [X] is the actual concentration of X at a given time. Only Ru^{2+}, BrO_3^-, and malonic acid were treated as inflow species. For all other variables $[X]_o = 0$. [e] The concentration of H_2O was kept constant at 55.5 M, and H^+ was treated as a parameter.

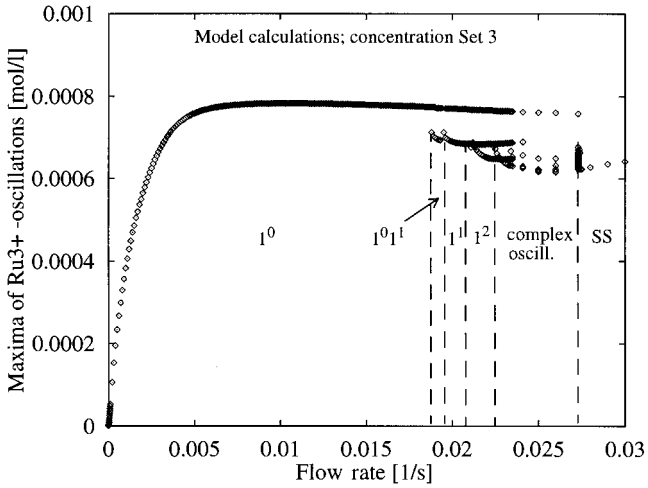

Figure 13. Model calculations; concentration set 3: Maxima of the oscillations versus flow rate. At low flow rates P1 oscillations are found while at high flow rates Farey-ordered complex periodic oscillations occur.

10^{-4} s^{-1} ($\tau = 166.7$ min) and 2.0×10^{-2} s^{-1} ($\tau = 0.8$ min) at intervals of $k_f = 1.0 \times 10^{-4}$ s^{-1}. They resulted in P1 oscillations at low flow rates. The bifurcation diagrams obtained for both concentration sets are similar to Figure 13. At high flow rates, Farey-ordered patterns occur. The oscillation periods show the same behavior as in the experiments. For concentration set 4 a maximum of the oscillation period (137 s) occurs at $k_f = 7.6$

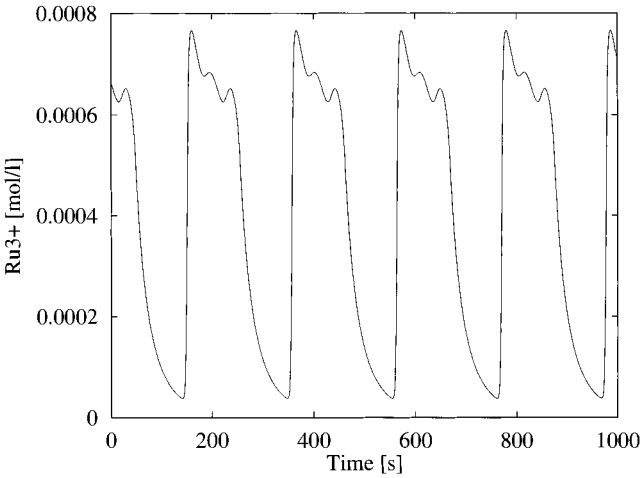

Figure 14. Model calculations; concentration set 3: Time series of P3 (1^2) state at $k_f = 2.20 \times 10^{-2}$ s^{-1} ($\tau = 0.76$ min).

$\times 10^{-3}$ s^{-1} ($\tau = 2.19$ min) while for concentration set 5 a minimum (35 s; $k_f = 1.0 \times 10^{-3}$ s^{-1}) of the oscillation periods precedes the maximum (72 s; $k_f = 1.03 \times 10^{-2}$ s^{-1}). The periods decrease with increasing bromate concentrations in agreement with the experiments. The Farey-ordered complex periodic oscillations are shifted to higher flow rates for increasing bromate concentrations. For example, a P3 (1^2) state is found at $k_f = 2.10 \times 10^{-2}$ s^{-1}, $k_f = 2.20 \times 10^{-2}$ s^{-1}, $k_f = 2.40 \times 10^{-2}$ s^{-1}, and $k_f = 2.70 \times 10^{-2}$ s^{-1} for concentration sets 2, 3, 4, and 5, respectively.

Discussion

The dynamics of the chemiluminescent BZ system is found to show some similarities with the well-known bifurcation behavior of the cerium-catalyzed BZ reaction.[12−15] The main difference between the ruthenium-catalyzed and the cerium-catalyzed reaction is that chaotic states are absent in the pure Ru system while the pure cerium-catalyzed system displays chaos. However, in the investigation of a cerium-rich mixture (mole fraction $Ru^{2+} = 0.05$), we could characterize two chaotic states C_1 and C_2 which are reached via a period-adding and a period-doubling route, respectively. The deterministic nature of the "period-doubling aperiodicity" C2 is evidenced by the Hausdorff dimension which is fractal ($D_H = 2.15$) and by an extremum in the corresponding one-dimensional map (Figure 12c). This chaotic state occurs at a flow rate different from that of chaos as observed under the same concentration conditions in the pure cerium-catalyzed reaction ($k_f = 4.8 \times 10^{-3}$s^{-1} and 3.2×10^{-4} s^{-1},[15] respectively). This indicates that the ruthenium complex is not a mere chemiluminescent indicator in the cerium system but it takes part in the chemical reaction.

For the other observed aperiodic state C1 an extremum in the one-dimensional map could not be observed. According to Shil'nikov[28] deterministic chaos may occur in a system which displays a homoclinic orbit biasymptotic to a saddle focus. The preceding period-adding scenario[29] and the associated increase of the oscillation periods[30] support the interpretation that this aperiodicity (C1) originates from a saddle focus which displays a biasymptotic orbit for $t \rightarrow -\infty$ and $t \rightarrow +\infty$. At the tip of the attractor the three coordinates in the Takens attractor are identical (Figure 8b), again supporting the notion that this point is located near an instable saddle focus.[30] A similar bifurcation scenario involving a period-adding route to homoclinic chaos has been observed recently in the peroxidase−oxidase reaction[31] which suggests that such scenarios may be generic. Experimental evidence for homoclinic chaos is already known in the pure cerium system.[32] At molar fractions of Ru^{2+} higher than ~0.5 the reaction dynamics approaches the dynamics of the pure ruthenium-catalyzed reaction which so far has shown only periodic states in the CSTR.

The extended model of Gao and Försterling[16] semiqualitatively describes the experimentally observed phenomena in the pure Ru system such as the bifurcation structure, the behavior of the oscillation amplitudes, and the oscillation periods for different concentration sets as well as the absence of chaos. It can be assumed that the Gao−Försterling model does not show any chaos (at least not in the investigated parameter range) because the feedback loop involving bromomalonic acid as a control species in the Györgyi−Field models[20] is replaced by a BrO_2-radical control. Only a small part of our simulations have been shown.

The standard redox potentials of Ce^{4+}/Ce^{3+} ($E_o = 1.44$ V) and $[Ru(bpy)_3]^{3+}/[Ru(bpy)_3]^{2+}$ ($E_o = 1.26$ V) are sufficiently different to affect the rates of the reactions in which the catalysts are involved. For example, the rate constants for reaction 6 (Table 1) are $k_6 = 4.0 \times 10^6$ L^2 mol^{-2} s^{-1} and $k_{-6} = 0$ for the ruthenium system and $k_6 = 6.2 \times 10^4$ L^2 mol^{-2} s^{-1} and $k_{-6} = 1.2 \times 10^4$ L mol^{-1} s^{-1} for the cerium system.[16] An important consequence is that a greater amount of catalyst is oxidized in the Ru system than in the Ce system.

The influence of the counterions chloride and sulfate on the reaction dynamics was also studied because chloride was shown to markedly influence the autocatalysis of the BZ system.[33] The chloride counterion leads to smaller oscillation amplitudes and shorter periods. It was further demonstrated that the choice of the chloride counterion is not the reason for the observed absence of complex periodic or chaotic states at low flow rates in the pure ruthenium system.

There is an interesting analogy to the peroxidase−oxidase reaction where the role of 2,4-dichlorophenol and other phenols and aromatic amines has been investigated recently.[34] In this reaction the occurrence of deterministic chaos is also significantly influenced by the choice of the phenol or aromatic amine as the electron carrier.[34] Complex periodic states such as the observed Farey-ordered states are well-known in the manganese-[35] and cerium-catalyzed BZ reaction.[14]

Acknowledgment. We thank Prof. Försterling, Dr. A. Münster, and Dr. M. Hauser for interesting discussions and Mr. M. Kraus for technical help. We further thank the Deutsche Forschungsgemeinschaft for financial support.

References and Notes

(1) Belousov, B. P. *Sb. Ref. Radiat. Med.* **1959**, 145; Zhabotinsky, A. M. *Biofizika* **1964**, *9*, 306. Field, R. J.; Burger, M. *Oscillations and Travelling Waves in Chemical Systems*; Wiley: New York, 1985.

(2) Bolletta, F.; Balzani, V. *J. Am. Chem. Soc.* **1982**, *104*, 4250.

(3) Gáspár, V.; Bazsa, G.; Beck, M. T. *Z. Phys. Chem. (Leipzig)* **1983,** *264*, 43; Jinguji, M.; Ishihara, M.; Nakazawa, T. *J. Phys. Chem.* **1992**, *96*, 4279; Sørensen, P. G.; Lorenzen, T.; Hynne, F. *J. Phys. Chem.* **1996**, *100*, 19192.

(4) Mori, Y.; Nakamichi, Y.; Sekiguchi, T.; Okazaki, N.; Matsumura, T.; Hanazaki, I. *Chem. Phys. Lett.* **1993**, *211*, 421.

(5) Srivastava, P. K.; Mori, Y.; Hanazaki, I. *Chem. Phys. Lett.* **1992**, *190*, 279.

(6) Kuhnert, L.; Agladze, T.; Krinsky, V. I. *Nature* **1989**, *337*, 244; Jinguji, M.; Ishihara, M.; Nakazawa, T. *J. Phys. Chem.* **1990**, *94*, 1226.

(7) Steinbock, O.; Zykov, V.; Müller, S. C. *Nature* **1993**, *366*, 322; Grill, S.; Zykov, V. S.; Müller, S. C. *Phys. Rev. Lett.* **1995**, *75*, 3368.

(8) Hercules, D. M.; Lytle, F. E. *J. Am. Chem. Soc.* **1966**, *88*, 4745.

(9) Tokel, N. E.; Bard, A. J. *J. Am. Chem. Soc.* **1972**, *94*, 2862.

(10) Rubinstein, I.; Bard, A. J. *J. Am. Chem. Soc.* **1981**, *103*, 512.

(11) Weigt, H. R. *Angew. Chem.* **1992**, *104*, 358.

(12) Turner, J. S.; Roux, J.-C.; McCormick, W. D.; Swinney, H. L. *Phys. Lett.* **1981**, *85A*, 9; Simoyi, R. H.; Wolf, A.; Swinney, H. L. *Phys. Rev. Lett.* **1982**, *49*, 245.
(13) Noszticzius, Z.; McCormick, W. D.; Swinney, H. L. *J. Phys. Chem.* **1987**, *91*, 5129; *J. Phys. Chem.* **1989**, *93*, 2796.
(14) Schneider, F. W.; Münster, A. F. *J. Phys. Chem.* **1991**, *95*, 2130.
(15) Hauser, M. J. B.; Schneider, F. W. *J. Chem. Phys.* **1994**, *100*, 1058; Zeyer, K.-P.; Münster, A. F.; Hauser, M. J. B.; Schneider, F. W. *J. Chem. Phys.* **1994**, *101*, 5126.
(16) Gao, Y.; Försterling, H.-D. *J. Phys. Chem.* **1995**, *99*, 8638.
(17) Försterling, H.-D.; Murányi, S.; Noszticzius, Z. *J. Phys. Chem.* **1990**, *94*, 2915.
(18) Györgyi, L.; Field, R. J.; Noszticzius, Z.; McCormick, W. D.; Swinney, H. L. *J. Phys. Chem.* **1992**, *96*, 1228.
(19) Försterling, H.-D. Personal communication.
(20) Györgyi, L.; Turányi, T.; Field, R. J. *J. Phys. Chem.* **1990**, *94*, 7162 and references therein.
(21) Hindmarsh, A. C. In *Scientific Computing*; Stepleman, R. S., et al., Eds.; North-Holland: Amsterdam, 1983; p 55.
(22) Kazakov, V. P.; Karavayev, A. D.; Vakhidova, S. R. *React. Kinet. Catal. Lett.* **1991**, *45*, 199.
(23) Farey, J. *Philos. Mag. J. (London)* **1816**, *47*, 385.
(24) Grill, S. Diplomarbeit, Universität Göttingen, 1995.
(25) Takens, F. In *Lecture Notes in Mathematics*; Rand, D. A., Young, L. S., Eds.; Springer: Berlin, 1981; p 366.
(26) Broomhead, D. S.; King, G. P. *Physica* **1986**, *20 D*, 217.
(27) Badii, R.; Politi, A. *Phys. Rev. Lett.* **1984**, *52*, 1661; van de Water, W.; Schram, P. *Phys. Rev.* **1988**, *37 A*, 3118.
(28) Shil′nikov, L. P. *Sov. Math. Dokl.* **1965**, *6*, 163.
(29) Swinney, H. L. *Physica* **1983**, *7 D*, 3; Gaspard, P.; Kapral, R.; Nicolis, G. *J. Stat. Phys.* **1984**, *35*, 697.
(30) Healey, J. J. *Physica* **1995**, *80 D*, 48.
(31) Hauser, M. J. B.; Olsen, L. F. *J. Chem. Soc., Faraday Trans.* **1996**, *92*, 2857.
(32) Argoul, F.; Arneodo, A.; Richetti, P. *Phys. Lett.* **1987**, *120A*, 269.
(33) Jacobs, S. S.; Epstein, I. R. *J. Am. Chem. Soc.* **1976**, *98*, 1721; Murányi, S.; Försterling, H.-D. *Z. Naturforsch.* **1990**, *45 A*, 135.
(34) Hauser, M. J. B.; Olsen, L. F. *Biochemistry* **1998**, *37*, 2458; Kummer, U.; Hauser, M. J. B.; Wegmann, K.; Olsen, L. F.; Baier, G. *J. Am. Chem. Soc.* **1997**, *119*, 2084.
(35) Maselko, J.; Swinney, H. L. *J. Chem. Phys.* **1986**, *85*, 6430.